

# Investigation of the in vitro corrosion behavior and biocompatibility of niobium (Nb)-reinforced hydroxyapatite (HA) coating on CoCr alloy for medical implants

Balraj Singh<sup>1</sup>, Gurpreet Singh<sup>1,a)</sup> , Buta Singh Sidhu<sup>2</sup>

<sup>1</sup>Department of Mechanical Engineering, Punjabi University, Patiala, Punjab 147002, India

<sup>2</sup>Dean of Planning and Development, MRS Punjab Technical University, Bathinda, Punjab 151001, India

<sup>a)</sup>Address all correspondence to this author. e-mail: gurpreetnabha@pbi.ac.in

Received: 28 December 2018; accepted: 27 February 2019

In this study, a niobium-reinforced hydroxyapatite (HA-Nb) coating was developed on cobalt–chromium (CoCr) alloy by plasma spraying with three varied levels, i.e., 10, 20, and 30% of weight percent (wt%) of Nb content. The corrosion behavior and biocompatibility of the samples were analyzed through electrochemical corrosion testing and cytotoxicity studies, respectively. The results of corrosion testing revealed that the HA coating increased the corrosion resistance of the CoCr alloy, and with the incremental increase of Nb reinforcement in HA, corrosion resistance was further enhanced. The HA-30Nb coating demonstrated the finest corrosion resistance with the highest  $E_{\text{corr}}$  and lowest  $I_{\text{corr}}$  values, which were about one order of magnitude lower in comparison to the bare CoCr alloy. The surface hardness increased and the surface roughness decreased with the increase of Nb content in the coating. Wettability analysis revealed that HA and HA-Nb coatings had a hydrophilic nature. HA-Nb coatings demonstrated a significantly better cell proliferation than the CoCr alloy.

## Introduction

Titanium alloys, stainless steel (SS), and CoCr alloys are the commonly used metallic biomaterials in biomedical implantology [1]. Among these biomaterials, CoCr alloys are widely used as orthopedic implants, particularly in dentistry and total joint replacements (TJR) because of their robust mechanical properties and wear resistance [2, 3]. However, the ions ( $\text{Co}^{2+}$ ,  $\text{Cr}^{3+}$ , and  $\text{Cr}^{6+}$ ) that release because of the excessive corrosion of CoCr alloys induce allergic reactions and can even cause DNA damage, necrosis, cell apoptosis, and chromosome breakage [4, 5]. Despite the advancements in medical and surgical therapies, the osteomyelitis (bone infection) rates after TJR procedures are still noticeable with 0.5–6% for total hip replacement (THR) and about 1.5% in total knee replacement (TKR) [6, 7]. It has been predicted that by the year 2030, there will be a rise of 174% and 673% in THR and TKR procedures, respectively [8]. Therefore, the need for improvements in the performance of the current generation of biomaterials is of prime importance and interest.

Calcium phosphate-based coating, especially HA ( $\text{Ca}_{10}(\text{PO}_4)_6(\text{OH})_2$ ), plays a crucial role in enhancing the corrosion resistance and biologic response of metallic biomaterials [9, 10]. There are various methods to produce HA coating on a metallic substrate, among which plasma spray technique is commercially well proven and approved by Food and Drug Administration (FDA, USA) [11]. In the earlier studies, HA coating had been deposited on CoCr alloys, mainly through sol-gel method and electrodeposition, to enhance their performance for bioimplant applications [12, 13, 14, 15, 16]. Several ceramic, polymer, and metallic secondary phases, such as ceria ( $\text{CeO}_2$ ), zirconia ( $\text{ZrO}_2$ ), calcium phosphate (CaP), silica ( $\text{SiO}_2$ ), titania ( $\text{TiO}_2$ ), polycaprolactide (PCL), magnesium oxide (MgO), zinc, strontium, and silver, etc., were also incorporated in HA to improve its properties for biomedical applications [17, 18, 19, 20, 21, 22, 23, 24, 25]. However, Nb has been scarcely studied in combination with HA as compared to other combinations mentioned above. Nb is considered as one of the safest metal that can be tolerated by the human body and

it possesses excellent corrosion resistance in aggressive environments [26, 27, 28]. Nonetheless, Nb is mechanically weak in its pure form [29]. Utilization of Nb as a coating constituent along with HA is one possible way to improve the corrosion resistance and biologic response of metallic biomaterials. The surface properties such as surface hardness, roughness, and wettability influence corrosion behavior and biological response of bioimplants; thus, the investigation of these properties is also very crucial [30].

In this study, the CoCr alloy was coated with HA, Nb, and HA-Nb coatings by varying the reinforcement of Nb at three levels, i.e., 10, 20, and 30 wt% (HA-10Nb, HA-20Nb, and HA-30Nb). Corrosion behavior and cytotoxicity of uncoated and coated samples were investigated along with the analysis of surface properties.

## Results and discussion

### Characterization

The scanning electron micrographs of HA and Nb powders are shown in Fig. 1. Particles of both the powders [Figs. 1(a) and 1(b)] had an irregular morphology. Figure 2 presents the X-ray diffraction (XRD) patterns of the feedstock powders. The analysis of the XRD patterns demonstrated the presence of HA and Nb powders in crystalline phases. The phases were identified by comparing the XRD patterns of HA and Nb with JCPDS card 9-432 and 35-0789, respectively. With an increase in the Nb content, the peak intensities corresponding to Nb

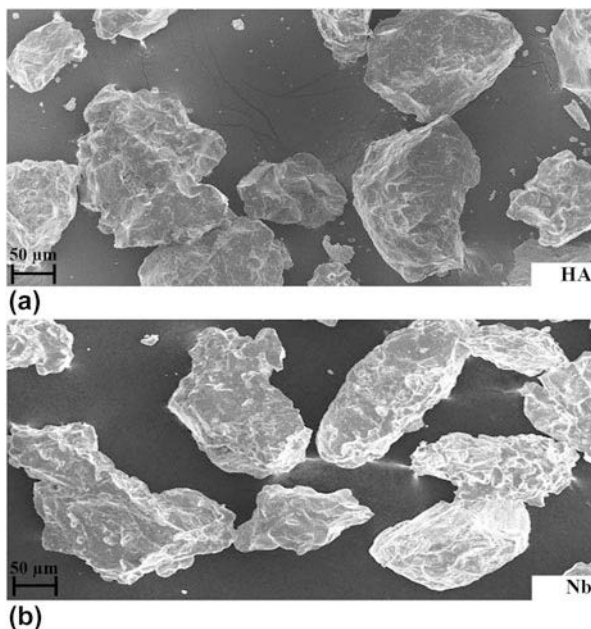


**Figure 1:** Scanning electron micrographs of (a) HA and (b) Nb powders.

were pronounced, whereas the HA phase maintained its identity.

Figure 3 shows the XRD patterns of different as-sprayed coatings. The amorphous hump corresponding to  $\beta$ -tricalcium phosphate ( $\beta$ -TCP; JCPDS card 9-169), peaks corresponding to tetracalcium phosphate (TTCP; JCPDS card 25-1137), and peaks corresponding to  $\alpha$ -tricalcium phosphate ( $\alpha$ -TCP; JCPDS card 9-348), as observed in the diffraction pattern HA-based coatings [Figs. 3(a) and 3(c)–3(e)], were also reported in earlier studies [31, 32]. During the plasma spraying process, the HA powder is melted at a very high temperature due to which HA is dehydroxylated as well as decomposed and amorphous phases commonly exist in the HA coating [33]. The presence of an amorphous phase is reported to be advantageous for the early integration of bioimplant to bone/cell tissue [30].

The peaks of Nb oxide phase (JCPDS card 30-0873) appear in the diffraction pattern of the Nb coating and in HA-Nb coatings [Figs. 3(b)–3(e)]. The earlier studies on Nb-based coatings revealed that the Nb oxide content was beneficial for the enhanced protection ability and biological response [34, 35, 36]. With the increase of Nb reinforcement in HA, the peaks of TTCP were reduced and the amorphous hump related to  $\beta$ -TCP also lowered. When the Nb reinforcement was increased, the overall intensity of HA peaks increased marginally. HA coating had 74.6% crystallinity of the HA phase, whereas HA-10Nb, HA-20Nb, and HA-30Nb coatings represented crystallinity of 77.4%, 80.5%, and 82.9%, respectively. The crystallinity value of the HA and HA-Nb coatings obtained in this study are consistent with the crystallinity values reported for plasma-sprayed HA coatings by other researchers [30, 33, 37]. Moreover, the proportion of crystalline HA phase in pure HA coating and HA-Nb coatings is in accordance with the ISO 13779-2 standard [38]. The variation in crystallinity of the HA and HA-Nb coatings could be due to the difference between the thermal conductivity of HA and Nb. The value of thermal conductivity for HA and Nb is 0.7 W/m K and 52 W/m K, respectively [39, 40]. It has been reported that when the reinforcement possesses significantly higher thermal conductivity, it allows slower cooling rate to neighboring HA region [41]. After plasma spraying, the decline in the crystallinity of HA phase is mainly caused by the rapid cooling rate [30]. The slower cooling rate because of the presence of Nb is a possible explanation for the higher proportion of crystalline HA phase in HA-Nb coatings.

Figure 4 presents the scanning electron micrographs of the surface of as-sprayed coatings. Figures 4(a) and 4(c) show the morphology of pure HA and HA-10Nb coating that mainly is composed of melt-resolidified, spheroidized and fine particles and a few accumulated splats. When the Nb content in HA was increased, well-flattened splats were

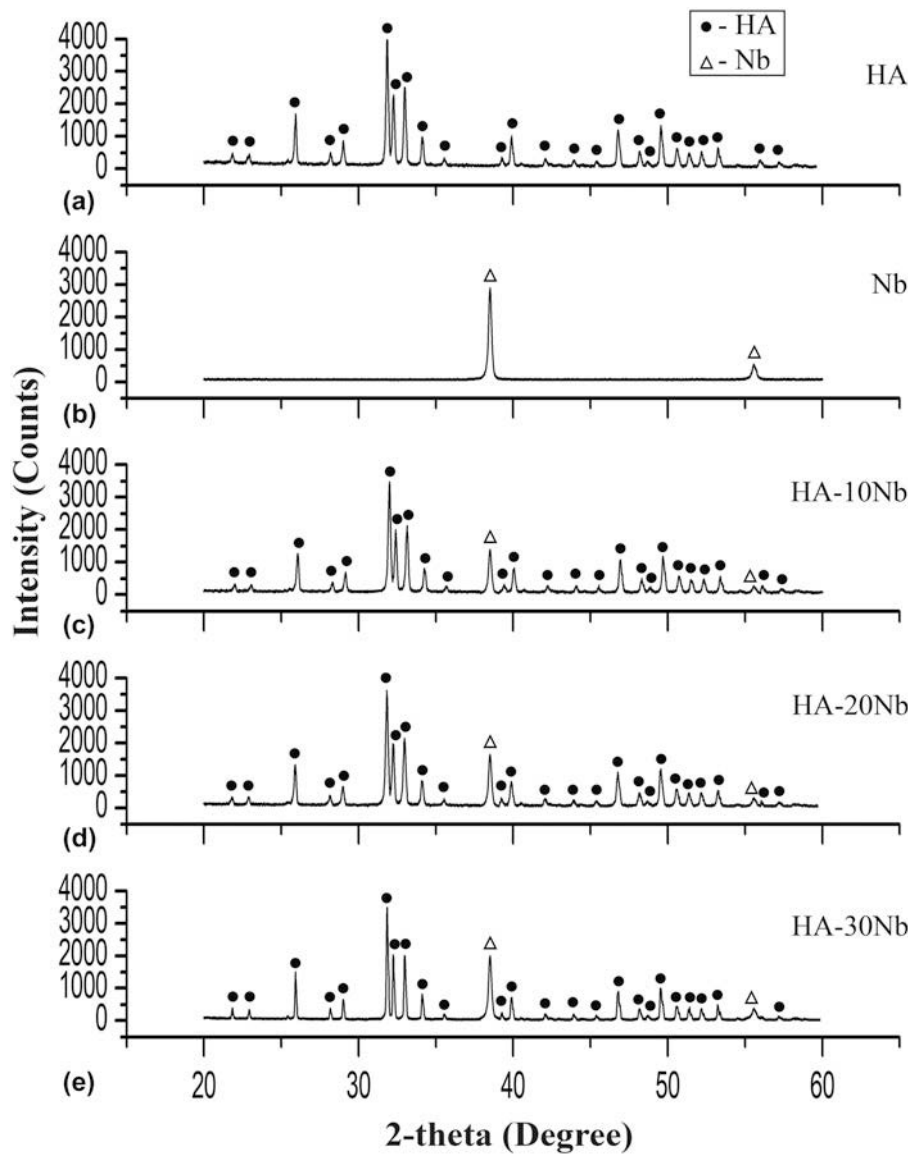


**Figure 2:** XRD patterns of (a) HA, (b) Nb, (c) HA-10Nb, (d) HA-20Nb, and (e) HA-30Nb spray powders.

observed at the surface of HA-20Nb and HA-30Nb coatings [Figs. 4(d) and 4(e)] and spheroidized particles were also reduced. The surface of the Nb coating [Fig. 4(b)] exhibited a relatively flat morphology but some microcracks were noticed at the surface. However, no prominent microcracks appeared at the surface of HA and HA-Nb coatings. The existence of the microcracks in the coating could result in rapid corrosion of the substrate material and also coating failure due to delamination because it facilitates direct contact between the substrate and body fluids [30].

The calcium–phosphorus ratio (Ca:P) of as-sprayed HA coating was 1.74 as determined by EDX analysis. The Ca:P did not fluctuate much with the reinforcement of Nb in HA, and Ca:P values of 1.71, 1.69, and 1.68 were observed for HA-10Nb,

HA-20Nb, and HA-30Nb coatings, respectively. Ellies et al. [42] reported that the Ca:P ratio ranging from 1.67 to 1.76 is ideal for HA-coated bioimplants. Furthermore, it is evident from the EDX analysis that the Nb reinforcement in HA-Nb coatings was uniformly distributed and lump formation of Nb reinforcement did not occur.

Figure 5 shows the scanning electron micrographs from the cross-section of as-sprayed coatings. In this figure, the area marked as ‘S,’ ‘C,’ and ‘E’ represents the substrate, coating, and epoxy region, respectively. The coatings exhibited almost uniform thickness of ~125 μm. The HA and Nb coating [Figs. 5(a) and 5(b)] were intact with the substrate as the substrate–coating interface was free from microcracking. Similarly, Nb-reinforced HA coatings [Figs. 5(c)–5(e)] revealed

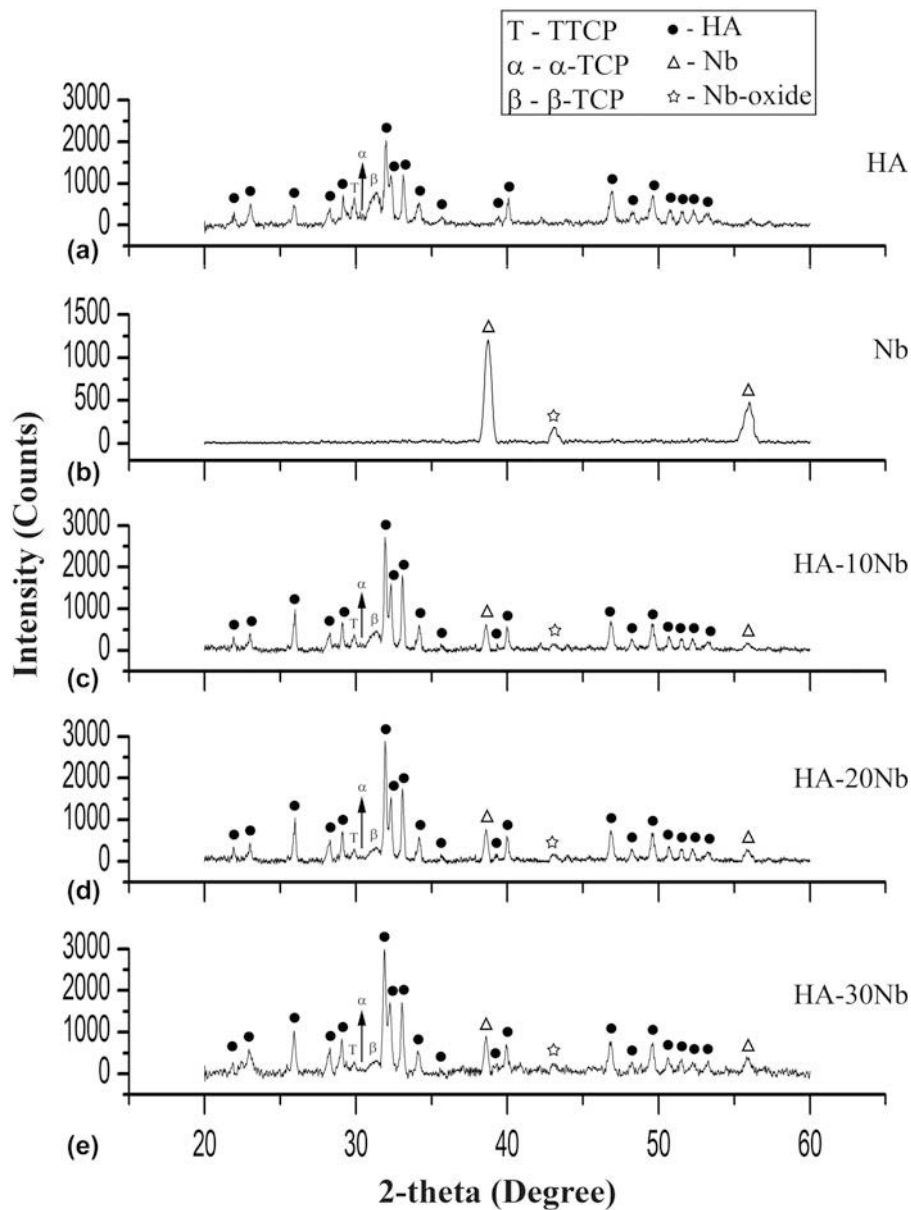


Figure 3: XRD patterns of as-sprayed (a) HA, (b) Nb, (c) HA-10Nb, (d) HA-20Nb, and (e) HA-30Nb coatings.

strong bonding with the substrate because no prominent microcrack appeared at the substrate–coating interface.

Among the mechanical properties, the hardness of the surface plays an important role in determining the quality of a coating [43]. Figure 6(a) demonstrates the value of microhardness for different surfaces. The surface of uncoated CoCr alloy and the Nb coating revealed significantly higher microhardness value ( $P < 0.05$ ) as compared to HA and HA-Nb coatings. Among all the samples, the microhardness value of HA coating was the lowest. With the Nb reinforcement, the value of microhardness of the surface enhanced significantly ( $P < 0.05$ ) as compared to HA coating. The increment in the microhardness value could be attributed to the formation of

a layered framework as a result of the uniform distribution of the Nb reinforcement. A similar increase in surface hardness of HA coating has also reportedly observed in the earlier investigations of reinforced HA coatings [32, 44]. The microhardness values of HA and HA-Nb coatings are comparable to the microhardness of HA coatings that have been reported in the earlier studies [32, 41, 45].

Figure 6(b) presents the average surface roughness ( $R_a$ ) value for the coated samples. The Nb-coated sample had the lowest surface roughness. HA coating had higher  $R_a$  value in comparison to Nb coating. The  $R_a$  values of HA and HA-10Nb coatings did not differ much. With the gradual increment of Nb content in HA, the  $R_a$  value was further

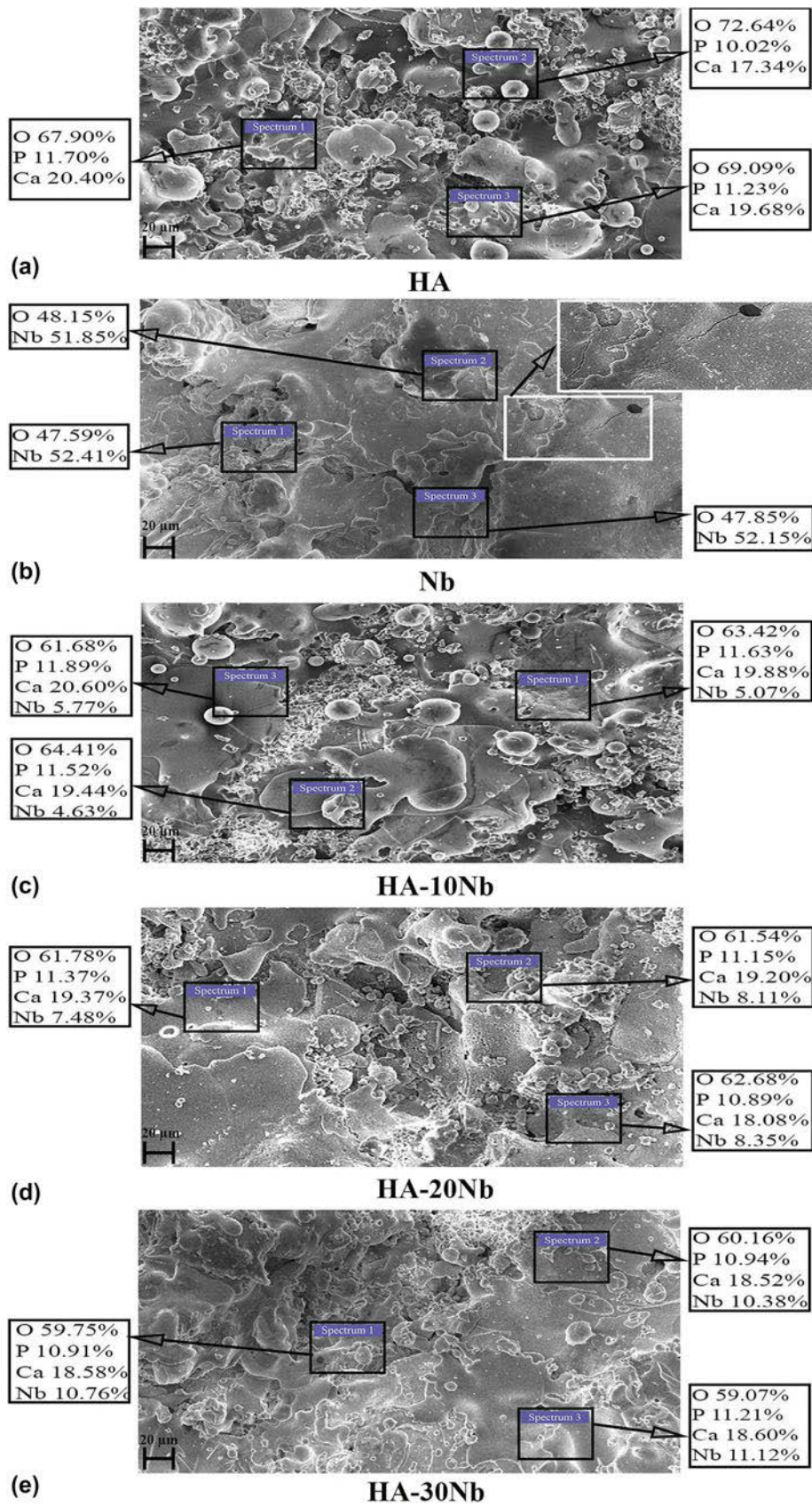


**Figure 4:** Scanning electron micrographs from the surface of as-sprayed (a) HA, (b) Nb, (c) HA-10Nb, (d) HA-20Nb, and (e) HA-30Nb coatings.

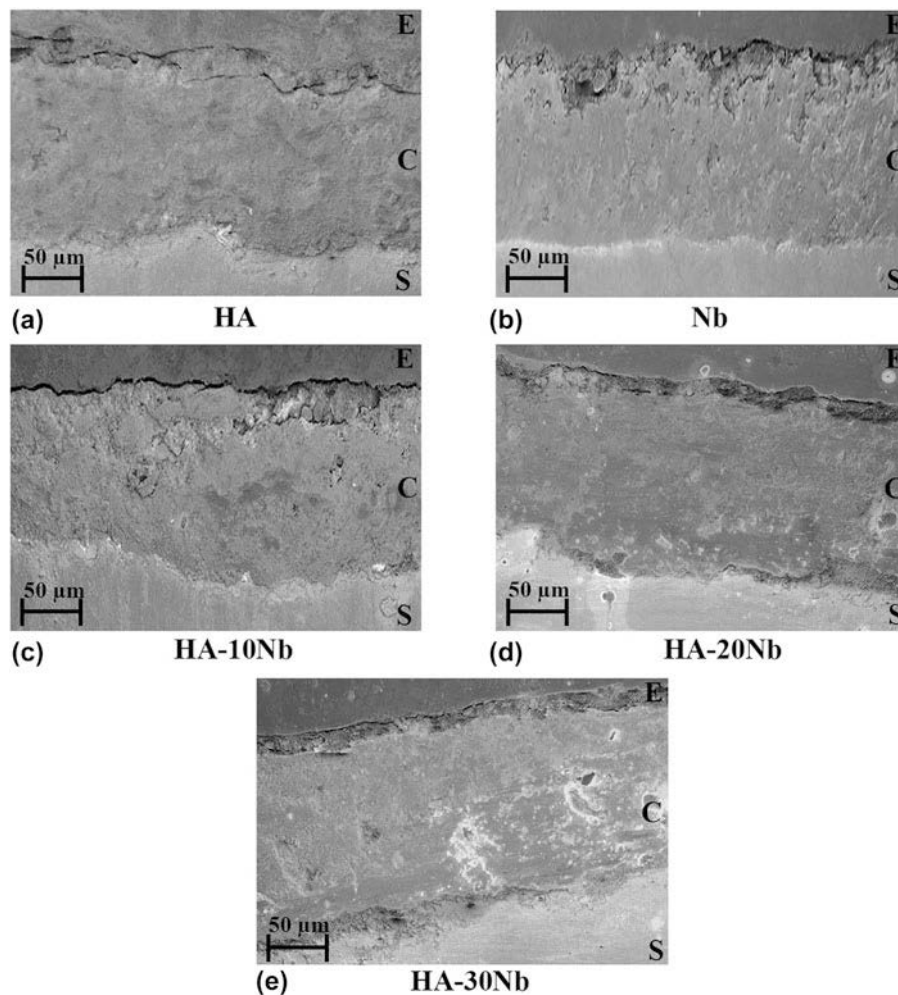


**Figure 5:** Cross-sectional scanning electron micrographs of as-sprayed (a) HA, (b) Nb, (c) HA-10Nb, (d) HA-20Nb, and (e) HA-30Nb coatings.

decreased ( $P < 0.05$ ) for HA-20Nb and HA-30Nb. It can also be observed in Figs. 4(a)–4(c) that with the increase of Nb reinforcement, the melt-resolidified particles lessened and the surface was relatively flattened. The earlier studies which investigated the relationship of surface roughness and the biologic response endorse that an adequate roughness at the surface of implants enhances its protein absorption, which results in better osteoconduction [46, 47]. The  $R_a$  values of HA and HA-Nb coatings are within the range for  $R_a$  values of plasma-sprayed HA coatings (2–6  $\mu\text{m}$ ) [48].

Wettability of the samples was evaluated from the contact angle values of the Ringer's solution droplet [Fig. 6(c)]. The CoCr alloy and Nb coating surface demonstrated hydrophobic nature, whereas the nature of the surface of HA coating was hydrophilic. The contact angle values increased ( $P < 0.05$ ) for HA-Nb coatings; however, the surface retained hydrophilic nature. The presence of a large amount of hydroxyl groups in the coating facilitates rapid absorption of the fluid that comes in contact with the surface [49], which could be the reason of

hydrophilic nature of HA and HA-Nb coatings. During the early stage of the contact between the cellular tissue and surface of an implant, the cells can be considered as a simple viscous fluid [50]. After the implantation, the adherence of the cells starts after the absorbance of blood proteins at the surface of the implant [51]. As per the literature, the contact angle value less than or equal to  $60^\circ$  is classified as the threshold value of hydrophilicity, and cell adherence was found to be favored for hydrophilic surfaces [52].

### Corrosion behavior analysis

Potentiodynamic polarization curves for different samples are displayed in Fig. 6(d). The electrochemical parameters derived from these curves through Tafel extrapolation are listed in Table I. Corrosion potential ( $E_{\text{corr}}$ ) and corrosion current density ( $I_{\text{corr}}$ ) are crucial parameters through which corrosion behavior of different samples is analyzed. A nobler  $E_{\text{corr}}$  value and lower  $I_{\text{corr}}$  value indicate superior corrosion resistance [53, 54].

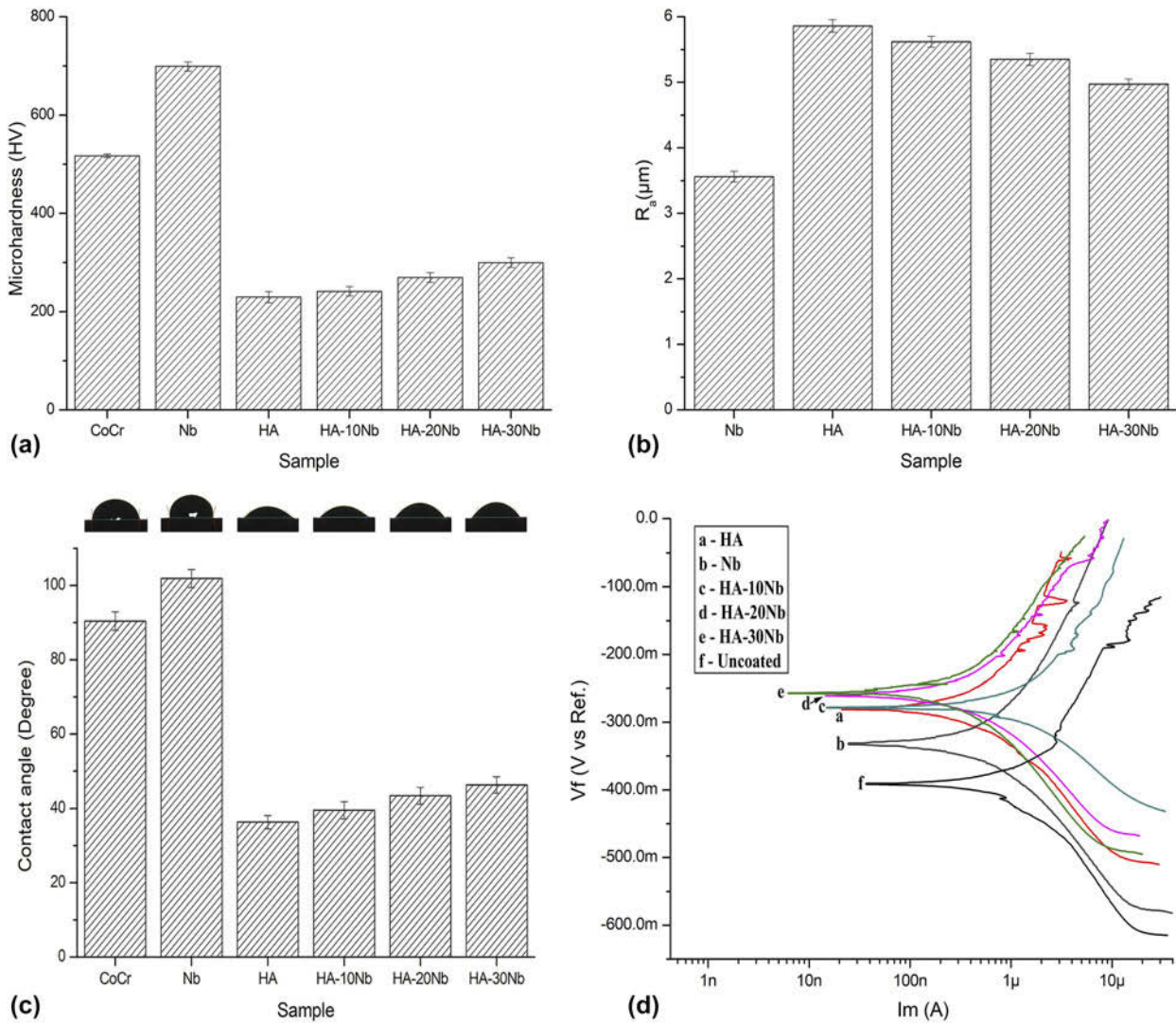


**Figure 6:** (a) Microhardness values of samples. (b)  $R_a$  values for coated samples. (c) Contact angle and droplet profile on the surface of samples. (d) Potentiodynamic polarization curves for different samples.

**TABLE I:** Corrosion parameters obtained through Tafel extrapolation.

Sample	$E_{corr}$ (mV)	$I_{corr}$ (per $cm^2$ )	$\beta_a$ ( $e^{-3}$ V/decade)	$\beta_c$ ( $e^{-3}$ V/decade)
Uncoated	-392	3.03 $\mu$ A	166	143
Nb	-331	456 nA	159	171
HA	-280	354 nA	175	148
HA-10Nb	-278	339 nA	181	143
HA-20Nb	-261	298 nA	169	143
HA-30Nb	-249	287 nA	162	196

The uncoated CoCr alloy and Nb-coated sample revealed lower  $E_{corr}$  as compared to the other samples. The  $E_{corr}$  value increased with HA coating, and with Nb reinforcement in HA,  $E_{corr}$  further shifted toward more noble values. The uncoated CoCr alloy exhibited the highest  $I_{corr}$  value among all the samples. The  $I_{corr}$  value of Nb-coated sample was lower in comparison to the uncoated sample but higher than the HA-

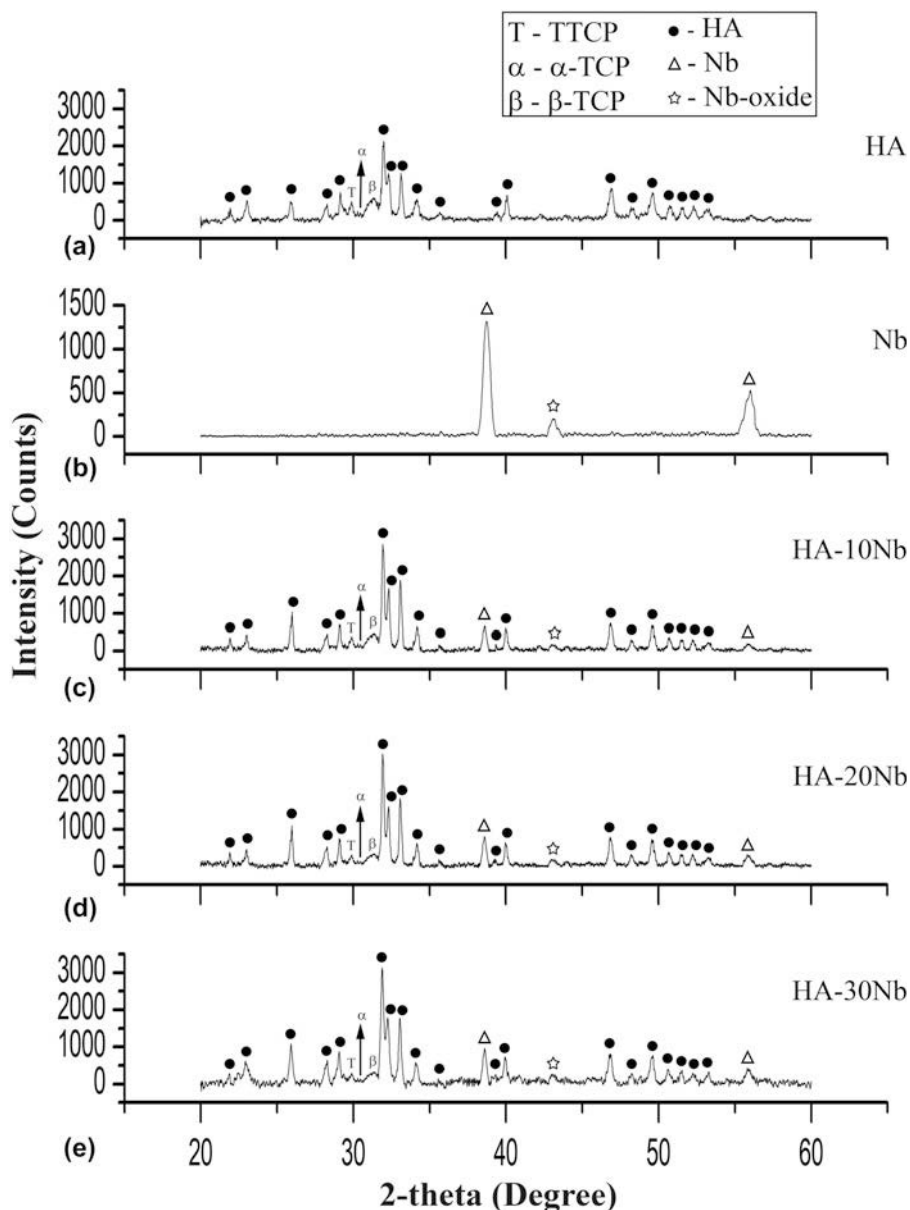
coated sample. Earlier studies that investigated the corrosion behavior of HA coatings on CoCr alloy also endorse that HA coating enhances passivation ability of the surface [11, 12, 13, 14]. The lower  $E_{corr}$  and higher  $I_{corr}$  values of Nb coating could be due to the presence of microcracks [Fig. 4(b)]. A structural defect in the coating, such as microcracking, promotes corrosion underneath the coating and at the surface, which results in the release of ions into the corrosive media and protection ability of the surface against corrosion [55]. Because of the incorporation of Nb in HA, the  $I_{corr}$  values declined further and the sample with HA-30Nb coating demonstrated lowest  $I_{corr}$ , which is about one order of magnitude lesser than the uncoated CoCr alloy. Enayati et al. [56] have also reported that a noteworthy increase in corrosion resistance of SS 316L was observed after HA-Nb coating. In this study, the fraction of crystalline HA phase increased and the value of  $I_{corr}$  decreased

with the increase of Nb content in HA. Reportedly, the corrosion resistance of the implants improves with the increase in the phase purity of HA coating [57]. Thus, the lower  $I_{corr}$  values, i.e., superior corrosion resistance of HA-Nb coatings could be attributed to their higher crystallinity of HA phase. The results obtained through electrochemical investigation are evident that the Nb reinforcement in HA increased the protection ability of the surface against corrosion, which could enhance long-term survivability of CoCr implants.

After the corrosion testing, XRD analysis of the coatings was done to analyze phase constituents [Fig. 7]. The results of XRD analysis demonstrated that formation/vanishing of any prominent phase did not occur after exposure to the Ringer's

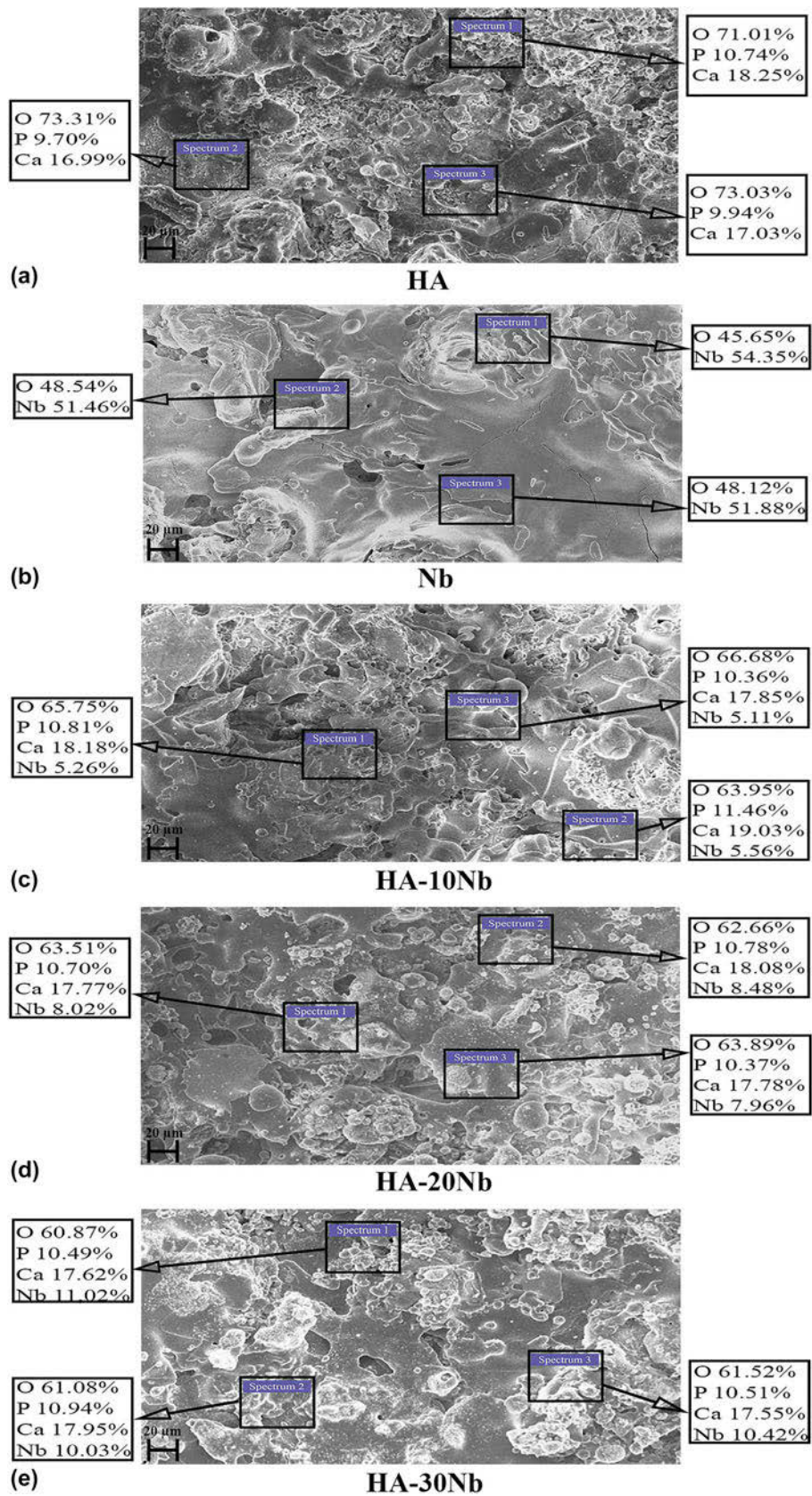
solution indicating that phase purity was retained by all the coatings. A marginal increment in the overall peak intensities of HA and HA-Nb coatings was observed. After corrosion testing, the crystallinity of HA phase in HA, HA-10Nb, HA-20Nb, and HA-30Nb coatings was 78.8%, 79.7%, 82.1%, and 84.2%, respectively. After the immersion in Ringer's solution, an increment in the phase purity of HA-based coatings is generally observed because of the dissipation of amorphous phases [58, 59]. The initial dissolution of HA enhances the growth of biological equivalents that promote mineralization of bone structure and bone formation [33].

Figure 8 presents the scanning electron micrographs of the coatings after corrosion testing. The microstructure of the pure



**Figure 7:** XRD patterns of (a) HA, (b) Nb, (c) HA-10Nb, (d) HA-20Nb, and (e) HA-30Nb coatings after corrosion testing in Ringer's solution.





**Figure 8:** Scanning electron micrographs from the surface of (a) HA, (b) Nb, (c) HA-10Nb, (d) HA-20Nb, and (e) HA-30Nb coatings after corrosion testing in Ringer's solution.

HA coating comprised primarily of the accumulated splats with a few flattened particles of asymmetrical morphology [Fig. 8(a)]. The microcracks became more notable at the surface of Nb coating [Fig. 8(b)] after corrosion testing. Morphology of the surface of HA-10Nb, HA-20Nb, and HA-30Nb coatings [Figs. 8(c)–8(e), respectively] after corrosion testing was dominated by well-flattened splats without any noticeable microcracking. It has been reported that the existence of a microcrack in the coating reduces corrosion protection ability of the surface and even coating failure/delamination can occur because of the microcracking [30, 60]. EDX analysis of all the samples was conducted to analyze the elemental composition of the coating surface after corrosion testing. After the exposure to the Ringer’s solution, a decrease in Ca:P was observed for HA and HA-Nb coatings. HA coating revealed Ca:P value of 1.72; whereas HA-10Nb, HA-20Nb, and HA-30Nb coatings

had Ca:P values 1.69, 1.68, and 1.66, respectively. The proportion of oxygen was increased for HA, HA-10Nb, HA-20Nb, and HA-30Nb coatings from 69.9%, 63.2%, 62%, and 59.7% to 72.4%, 65.5%, 63.4%, and 61.2%, respectively. Previous studies of HA coating have reported a similar decrease in Ca:P and increment in oxygen content as observed in the present investigation [18, 20, 60]. The osseointegration has also reportedly enhanced by the increase in oxygen content of the coating [54].

**Biocompatibility analysis**

The biocompatibility of the samples was tested on MG-63 cells. Cells were directly exposed to the samples as indicated. Cell proliferation (MTS) data are shown in Figs. 9(a) and 9(b) in which asterisk (\*) denotes significance, i.e., *P*-value < 0.05. After 72-h incubation [Fig. 9(a)], no cytotoxic effect was

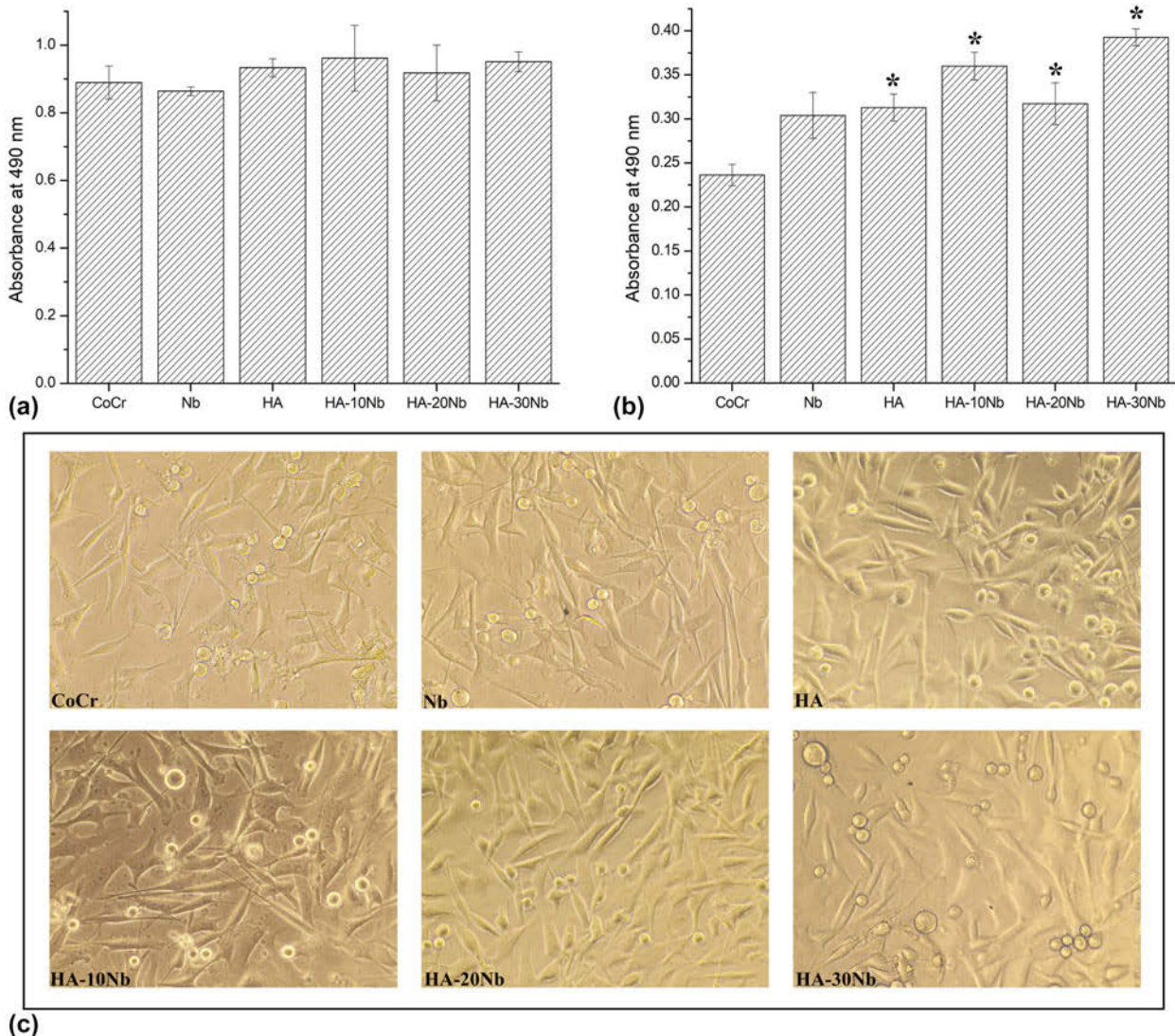


**Figure 9:** Cell proliferation (MTS) data after (a) 72-h incubation and (b) 96-h incubation; (c) cell health after 96-h incubation with different samples.

observed for coated samples as compared to CoCr alloy, and cell proliferation for the uncoated and coated CoCr samples was not significantly different. Further, after 96 h [Fig. 9(b)], an increase in cell proliferation was observed for HA-coated sample. The pure Nb-coated sample revealed almost same cell proliferation as the uncoated CoCr alloy. These results demonstrate that the surface of HA coating was more conducive to cell proliferation than the CoCr alloy and Nb coating. Reportedly, HA coating outperforms the metallic surfaces in biocompatibility because it possesses similarities to the mineral phase of the human bone [15]. With the Nb reinforcement in HA coating, no cytotoxic effect was observed on MG-63 cells, and a significant increase in cell proliferation was observed for HA-10Nb, HA-20Nb, and HA-30Nb coatings as compared to CoCr alloy. The crystallinity of HA phase is a critical parameter, which influences the biologic response of the coating surface [61]. The crystallinity of HA phase in HA-Nb coatings was higher than the pure HA coating, which could be the reason that HA-Nb coatings revealed relatively higher cell proliferation as compared to pure HA coating. Microscopic studies of cells exposed to the samples for 96 h revealed no changes in the morphology of the cells [Fig. 9(c)], indicating that the coatings do not have cytotoxic effect.

All in all, the results of the present investigation showed that the Nb reinforcement in HA increased the protection ability of the surface against corrosion and promoted cell proliferation, which could enhance long-term survivability and biologic response of the CoCr implants.

## Conclusions

In conclusion, plasma spray technique was used to deposit HA, Nb, HA-10Nb, HA-20Nb, and HA-30Nb coatings on the CoCr alloy ASTM F-1537. XRD results demonstrated that the fraction of crystalline HA phase increased as the Nb content was increased in the HA. Scanning electron microscopy (SEM) analysis revealed that microcracking was not observed at the surface and cross-section of as-sprayed HA and HA-Nb coatings, whereas microcracks appeared at the surface of Nb coating. The surface hardness of the HA coating was increased with the incremental increase of Nb reinforcement and the surface roughness decreased as the Nb reinforcement increased. The surface of CoCr alloy and Nb coating demonstrated hydrophobic properties; however, HA and HA-Nb coatings displayed hydrophilic nature of the surface. Both HA coating and Nb coating enhanced the corrosion resistance of CoCr alloy, whereas Nb-coated sample revealed the lowest corrosion resistance among all the coated samples. The values of  $I_{\text{corr}}$  decreased and  $E_{\text{corr}}$  became nobler with the incremental increase of Nb reinforcement in HA. HA-30Nb coating exhibited preeminent corrosion resistance with the noblest  $E_{\text{corr}}$  and lowest  $I_{\text{corr}}$  values, which

were about one order of magnitude lower as compared to the uncoated CoCr alloy. HA-Nb coatings revealed a significant increase in cell proliferation as compared to the uncoated CoCr alloy and demonstrated no cytotoxic effect on MG-63 cells. The results of this study suggest that Nb-reinforced HA coatings could be potentially used to enhance the corrosion resistance and biocompatibility of CoCr implants and thus deserve further biological investigation.

## Experimental setup

### Deposition of Coatings

Plasma-sprayed coatings of HA, Nb, HA-10Nb, HA-20Nb, and HA-30Nb were prepared using the MF4 plasma spray gun (MEC Pvt., Ltd., Jodhpur, India). An arc current of 600 amperes with 63 volts of arc voltage was used for plasma spraying. Argon and hydrogen were used as primary and secondary gas with the flow rate of 40 SLPM and 5 SLPM, respectively. Spraying distance for the process was kept 75 mm. Spray powders of HA and Nb were supplied by Medicoat, Etupes, France and BGY Science and Technology Co., Ltd., Beijing, China, respectively. A jar mill was used to prepare the mixtures of HA and Nb powders, which were used as spray feedstock. The medical grade CoCr alloy ASTM F-1537 (Zapp Precision Metals, Schwerte, Germany) of dimensions  $\varnothing$  15 mm  $\times$  5 mm was used as substrate material. To generate a rough surface, the substrates were grit blasted with alumina particles before the plasma spraying, and then air blasting of the substrates was performed to remove residual grit. The surface of CoCr substrates had an average surface roughness ( $R_a$ ) value of  $1.16 \pm 0.2$  after air blasting.

### Characterization techniques

Phase identification of the coatings was conducted using X-ray diffraction (XRD) analysis (X'Pert Pro Panalytical PN-3040/80, Almelo, Netherlands) over  $20^\circ$ – $60^\circ$  two-theta ( $2\theta$ ) range. The percentage amount of crystalline HA phase in different coatings was estimated as in an earlier study [31]. Scanning electron microscopy (SEM; JEOL JSM-6610LV, Akishima, Japan) equipped with EDX was used for the microstructural and compositional analyses of the coated surfaces before and after corrosion testing. The samples were coated with a thin layer of gold before the SEM/EDX analysis to obtain the desired conductivity of the surface. The substrate-coating interface was also analyzed through the SEM analysis. The sample preparation for cross-sectional SEM analysis was done by cutting the coated samples across the cross-section using a low-speed precision saw. Afterward, the samples were mounted in epoxy resin and polished with emery papers up to 2000 grade. Subsequently, buffing of the samples was

conducted using alumina slurry on the napped cloth to obtain a mirror finish.

A microhardness tester (Wolpert Wilson 402MVD, Aachen, Germany) was used to determine the value of microhardness from the polished cross-section of the coatings. The microhardness testing was conducted using a load of 50 gf for a dwell time of 15 s. The contact type profilometer (Mitutoyo SJ-210, Kamasaki, Japan) was used to analyze the roughness of the surfaces. The wettability of the samples was evaluated with a goniometer (First Ten Angstroms FTA2000, Portsmouth, New Hampshire) by measuring the contact angle of Ringer's solution droplet. For each surface property, an average of fifteen readings has been reported, and the data are expressed in the form of mean  $\pm$  standard deviation. The statistical analysis of the data has been conducted using Student's two-tailed *t*-test with a *P*-value  $< 0.05$  as statistical significance.

### Corrosion behavior analysis

The electrochemical corrosion testing was performed using a Potentiostat/Galvanostat/ZRA (Gamry G-750, Warminster, Pennsylvania). The potentiodynamic polarization studies were conducted using a standard three-electrode cell with Ag/AgCl (saturated KCl), graphite rod, and uncoated/coated sample serving as the reference, counter, and working electrode, respectively. As an electrolyte, Ringer's solution (Nice Chemicals Pvt., Ltd., Kochi, India) was used for simulating fluid conditions of the human body. To attain a relatively steady state, each sample was immersed in Ringer's solution for 24 h before the corrosion testing. Potentiodynamic scan was executed from an initial potential of  $-0.25$  V to final potential  $0.25$  V with scan rate of  $0.5$  mV/s. The values of electrochemical parameters were acquired from the potentiodynamic curve using Echem Analyst software (Gamry Instruments, Warminster, Pennsylvania).

### Biocompatibility investigation

The absence of cytotoxicity for all the samples was analyzed via in vitro cytotoxicity studies. Cytotoxicity of the samples was analyzed on MG-63 cells (osteoblast-like adherent cells), which were procured from the National Center for Cell Science (NCCS), Pune, India. Cells were cultured in Gibco RPMI 1640 media supplemented with 10% (V/V) fetal bovine serum (Gibco -Thermo Fisher, Waltham, Massachusetts) and 1% Penicillin-Streptomycin (Gibco -Thermo Fisher, Waltham, Massachusetts) at  $37$  °C in a humidified incubator at 5%  $\text{CO}_2$ . The samples were autoclaved before the analysis. Cells were grown at a seeding density of 8000 cells/well for 72-h incubation and of 6000 cells/well for 96-h incubation along with the samples in a 12-well plate. The uncoated CoCr alloy sample was used as the control. Media and samples were

removed from the 12-well plate after 72- or 96-h incubation, and cells were washed with 2 mL DPBS solution (Gibco -Thermo Fisher, Waltham, Massachusetts). After washing, the cells were trypsinized with 80  $\mu\text{L}$  of 0.25% Trypsin-EDTA (Gibco -Thermo Fisher, Waltham, Massachusetts) and neutralized with 300  $\mu\text{L}$  of fresh media/well. The suspended cells were then seeded into 96-well plate as triplicates (100  $\mu\text{L}$ /well). MTS assay (Promega Celltiter 96, Madison, Wisconsin) was done after 12-h incubation in 96-well plate. Spectrophotometrical absorbance was determined by a microplate reader (BMG LABTECH CLARIOstar, Ortenberg, Germany) at 490 nm. The qualitative analysis of cell health was conducted through the digital inverted microscope (Thermo Fisher EVOS XL, Waltham, Massachusetts).

### Acknowledgment

Zapp Precision Metals, Germany and Medicoat, France are gratefully acknowledged for sponsoring CoCr alloy substrate material and HA powder, respectively. The authors are also grateful to the Mechanical Engineering Department and Center for Biomedical Engineering, IIT Ropar, India for providing research facilities.

### References

1. **F. Likibi, B. Jiang, and B. Li:** Biomimetic nanocoating promotes osteoblast cell adhesion on biomedical implants. *J. Mater. Res.* **23**, 3222 (2008).
2. **H. Sahasrabudhe, S. Bose, and A. Bandyopadhyay:** Laser processed calcium phosphate reinforced CoCrMo for load-bearing applications: Processing and wear induced damage evaluation. *Acta Biomater.* **66**, 118 (2018).
3. **D. Cetiner, A.H. Paksoy, O. Tazegul, M. Baydogan, H. Guleryuz, H. Cimenoglu, and E. Atar:** A novel fabrication method for a  $\text{TiO}_2$  layer over CoCr alloy. *Surf. Eng.* **35**, 234 (2018).
4. **D. Pradhan, A.W. Wren, S.T. Misture, and N.P. Mellott:** Investigating the structure and biocompatibility of niobium and titanium oxides as coatings for orthopedic metallic implants. *Mater. Sci. Eng., C* **58**, 918 (2016).
5. **L. Luo, A. Petit, J. Antoniou, D.J. Zukor, O.L. Huk, R.C.W. Liu, F.M. Winnik, and F. Mwale:** Effect of cobalt and chromium ions on MMP-1, TIMP-1, and TNF- $\alpha$  gene expression in human U937 macrophages: A role for tyrosine kinases. *Biomaterials* **26**, 5587 (2005).
6. **H. Darwiche, W.K. Barsoum, A. Klika, V.E. Krebs, and R. Molloy:** Retrospective analysis of infection rate after early reoperation in total hip arthroplasty. *Clin. Orthop. Relat. Res.* **468**, 2392 (2010).
7. **K.L. Garvin and B.S. Konigsberg:** Infection following total knee arthroplasty: Prevention and management. *J. Bone Jt. Surg.* **93**, 1167 (2011).

8. N. Logan, A. Sherif, A.J. Cross, S.N. Collins, A. Traynor, L. Bozec, I.P. Parkin, and P. Brett: TiO<sub>2</sub>-coated CoCrMo: Improving the osteogenic differentiation and adhesion of mesenchymal stem cells in vitro. *J. Biomed. Mater. Res., Part A* **103**, 1208 (2015).
9. B. Singh, G. Singh, and B.S. Sidhu: Analysis of corrosion behavior and surface properties of plasma-sprayed HA/Ta coating on CoCr alloy. *J. Therm. Spray Technol.* **27**, 1401 (2018).
10. I. Ratha, A. Anand, S. Chatterjee, B. Kundu, and G.S. Kumar: Preliminary study on effect of nano-hydroxyapatite and mesoporous bioactive glass on DNA. *J. Mater. Res.* **33**, 1592 (2018).
11. A.A. Campbell: Bioceramics for implant coatings. *Mater. Today* **6**, 26 (2003).
12. T. Moskalewicz, A. Łukaszczyk, A. Kruk, M. Kot, D. Jugowiec, B. Dubiel, and A. Radziszewska: Porous HA and nanocomposite nc-TiO<sub>2</sub>/HA coatings to improve the electrochemical corrosion resistance of the Co–28Cr–5Mo alloy. *Mater. Chem. Phys.* **199**, 144 (2017).
13. M. İbrahim Coşkun, İ.H. Karahan, and Y. Yücel: Optimized electrodeposition concentrations for hydroxyapatite coatings on CoCrMo biomedical alloys by computational techniques. *Electrochim. Acta* **150**, 46 (2014).
14. M.R. Shirdar, S. Izman, M.M. Taheri, M. Assadian, and M. R. Abdul Kadir: Effect of electrophoretic deposition parameters on the corrosion behavior of hydroxyapatite-coated cobalt–chromium using response surface methodology. *Arabian J. Sci. Eng.* **41**, 591 (2016).
15. H. Kheimehsari, S. Izman, and M.R. Shirdar: Effects of HA-coating on the surface morphology and corrosion behavior of a Co–Cr-based implant in different conditions. *J. Mater. Eng. Perform.* **24**, 2294 (2015).
16. J.N. Barry, A. Cowley, P.J. McNally, and D.P. Dowling: Influence of substrate metal alloy type on the properties of hydroxyapatite coatings deposited using a novel ambient temperature deposition technique. *J. Biomed. Mater. Res., Part A* **102**, 871 (2014).
17. G. Singh, H. Singh, and B.S. Sidhu: Corrosion behavior of plasma sprayed hydroxyapatite and hydroxyapatite-silicon oxide coatings on AISI 304 for biomedical application. *Appl. Surf. Sci.* **284**, 811 (2013).
18. T.P. Singh, H. Singh, and H. Singh: Characterization, corrosion resistance, and cell response of high-velocity flame-sprayed HA and HA/TiO<sub>2</sub> coatings on 316L SS. *J. Therm. Spray Technol.* **21**, 917 (2012).
19. Y. Xiong, X. Hu, and R. Song: Characteristics of CeO<sub>2</sub>/ZrO<sub>2</sub>-HA composite coating on ZK60 magnesium alloy. *J. Mater. Res.* **32**, 1073 (2017).
20. G. Singh, H. Singh, and B.S. Sidhu: Characterization and corrosion resistance of plasma sprayed HA and HA–SiO<sub>2</sub> coatings on Ti–6Al–4V. *Surf. Coat. Technol.* **228**, 242 (2013).
21. Y. Huang, X. Zhang, H. Qiao, M. Hao, H. Zhang, Z. Xu, X. Zhang, X. Pang, and H. Lin: Corrosion resistance and cytocompatibility studies of zinc-doped fluorohydroxyapatite nanocomposite coatings on titanium implant. *Ceram. Int.* **42**, 1903 (2016).
22. V.V. Anusha Thampi and B. Subramanian: Enhancement of bioactivity of pulsed magnetron sputtered TiC<sub>x</sub>N<sub>y</sub> with bioactive glass (BAG) incorporated polycaprolactone (PCL) composite scaffold. *J. Alloys Compd.* **649**, 1210 (2015).
23. G. Singh, H. Singh, and B.S. Sidhu: In vitro corrosion investigations of plasma-sprayed hydroxyapatite and hydroxyapatite-calcium phosphate coatings on 316L SS. *Bull. Mater. Sci.* **37**, 1519 (2014).
24. D. Ke, S. Robertson, W. Dernel, A. Bandyopadhyay, and S. Bose: Effects of MgO and SiO<sub>2</sub> on plasma-sprayed hydroxyapatite coating: An in vivo study in rat distal femoral defects. *ACS Appl. Mater. Interfaces* **9**, 25731 (2017).
25. G. Fielding, M. Roy, A. Bandyopadhyay, and S. Bose: Antibacterial and biological characteristics of silver containing and strontium doped plasma sprayed hydroxyapatite coatings. *Acta Biomater.* **8**, 144 (2012).
26. S.A. Pauline and N. Rajendran: Effect of Sr on the bioactivity and corrosion resistance of nanoporous niobium oxide coating for orthopaedic applications. *Mater. Sci. Eng., C* **36**, 194 (2014).
27. M. Sowa, A. Kazek-Kesik, A. Krzakala, R.P. Socha, G. Dercz, J. Michalska, and W. Simka: Modification of niobium surfaces using plasma electrolytic oxidation in silicate solutions. *J. Solid State Electrochem.* **18**, 3129 (2014).
28. A. Robin and J.L. Rosa: Corrosion behavior of niobium, tantalum and their alloys in hot hydrochloric and phosphoric acid solutions. *Int. J. Refract. Met. Hard Mater.* **18**, 13 (2000).
29. M.H. Fathi and F. Azam: Novel hydroxyapatite/tantalum surface coating for metallic dental implant. *Mater. Lett.* **61**, 1238 (2007).
30. L. Sun, C.C. Berndt, K.A. Gross, and A. Kucuk: Material fundamentals and clinical performance of plasma-sprayed hydroxyapatite coatings: A review. *J. Biomed. Mater. Res.* **58**, 570 (2001).
31. L. Sun, C.C. Berndt, and C.P. Grey: Phase, structural and microstructural investigations of plasma sprayed hydroxyapatite coatings. *Mater. Sci. Eng., A* **360**, 70 (2003).
32. G. Singh, S. Singh, and S. Prakash: Surface characterization of plasma sprayed pure and reinforced hydroxyapatite coating on Ti6Al4V alloy. *Surf. Coat. Technol.* **205**, 4814 (2011).
33. T.P. Ntsoane, M. Topic, and R. Bucher: Near-surface in vitro studies of plasma sprayed hydroxyapatite coatings. *Powder Diffr.* **26**, 138 (2011).
34. H. Ardelean, I. Frateur, and P. Marcus: Corrosion protection of magnesium alloys by cerium, zirconium and niobium-based conversion coatings. *Corros. Sci.* **50**, 1907 (2008).

35. **S. Nagarajan, V. Raman, and N. Rajendran:** Synthesis and electrochemical characterization of porous niobium oxide coated 316L SS for orthopedic applications. *Mater. Chem. Phys.* **119**, 363 (2010).
36. **S.A. Pauline and N. Rajendran:** Biomimetic novel nanoporous niobium oxide coating for orthopaedic applications. *Appl. Surf. Sci.* **290**, 448 (2014).
37. **P.S. Prevéy:** X-ray diffraction characterization of crystallinity and phase composition in plasma-sprayed hydroxyapatite coatings. *J. Therm. Spray Technol.* **9**, 369 (2000).
38. **C. Zhang, H. Xu, X. Geng, J. Wang, J. Xiao, and P. Zhu:** Effect of spray distance on microstructure and tribological performance of suspension plasma-sprayed hydroxyapatite–titania composite coatings. *J. Therm. Spray Technol.* **25**, 1255 (2016).
39. **R.K. Williams, W.H. Butler, R.S. Graves, and J.P. Moore:** Experimental and theoretical evaluation of the phonon thermal conductivity of niobium at intermediate temperatures. *Phys. Rev. B* **28**, 6316 (1983).
40. **A. Rapacz-Kmita, A. Ślósarczyk, Z. Paszkiewicz, and D. Paluch:** Evaluation of HAp–ZrO<sub>2</sub> composites and monophasic HAp bioceramics. In vitro study. *J. Mater. Sci.* **39**, 5865 (2004).
41. **X. Chen, B. Zhang, Y. Gong, P. Zhou, and H. Li:** Mechanical properties of nanodiamond-reinforced hydroxyapatite composite coatings deposited by suspension plasma spraying. *Appl. Surf. Sci.* **439**, 60 (2018).
42. **L.G. Ellies, D.G.A. Nelson, and J.D.B. Featherstone:** Crystallographic changes in calcium phosphates during plasma-spraying. *Biomaterials* **13**, 313 (1992).
43. **M.F. Hasan, J. Wang, and C. Berndt:** Determination of the mechanical properties of plasma-sprayed hydroxyapatite coatings using the knoop indentation technique. *J. Therm. Spray Technol.* **24**, 865 (2015).
44. **D. Gopi, A. Karthika, D. Rajeswari, L. Kavitha, R. Pramod, and J. Dwivedi:** Investigation on corrosion protection and mechanical performance of minerals substituted hydroxyapatite coating on HELCDEB-treated titanium using pulsed electrodeposition method. *RSC Adv.* **4**, 34751 (2014).
45. **M.F. Hasan, J. Wang, and C. Berndt:** Evaluation of the mechanical properties of plasma sprayed hydroxyapatite coatings. *Appl. Surf. Sci.* **303**, 155 (2014).
46. **D. Yamashita, M. Machigashira, M. Miyamoto, H. Takeuchi, K. Noguchi, Y. Izumi, and S. Ban:** Effect of surface roughness on initial responses of osteoblast-like cells on two types of zirconia. *Dent. Mater. J.* **28**, 461 (2009).
47. **F.A. Shah, M.L. Johansson, O. Omar, H. Simonsson, A. Palmquist, and P. Thomsen:** Laser-modified surface enhances osseointegration and biomechanical anchorage of commercially pure titanium implants for bone-anchored hearing systems. *PLoS One* **11**, e0157504 (2016).
48. **K.A. Gross and M. Babovic:** Influence of abrasion on the surface characteristics of thermally sprayed hydroxyapatite coatings. *Biomaterials* **23**, 4731 (2002).
49. **W. Xie, J. Wang, C. Berndt, W. Xie, J. Wang, and C.C. Berndt:** Ethylene methacrylic acid (EMAA) single splat morphology. *Coatings* **3**, 82 (2013).
50. **Z. Geng, R. Wang, X. Zhuo, Z. Li, Y. Huang, L. Ma, Z. Cui, S. Zhu, Y. Liang, Y. Liu, H. Bao, X. Li, Q. Huo, Z. Liu, and X. Yang:** Incorporation of silver and strontium in hydroxyapatite coating on titanium surface for enhanced antibacterial and biological properties. *Mater. Sci. Eng., C* **71**, 852 (2017).
51. **F. Marashi-Najafi, J. Khalil-Allafi, and M.R. Etmannfar:** Biocompatibility of hydroxyapatite coatings deposited by pulse electrodeposition technique on the Nitinol superelastic alloy. *Mater. Sci. Eng., C* **76**, 278 (2017).
52. **S. Durdu, K. Korkmaz, S.L. Aktuğ, and A. Çakır:** Characterization and bioactivity of hydroxyapatite-based coatings formed on steel by electro-spark deposition and micro-arc oxidation. *Surf. Coat. Technol.* **326**, 111 (2017).
53. **M. Poorraeisi and A. Afshar:** The study of electrodeposition of hydroxyapatite–ZrO<sub>2</sub>–TiO<sub>2</sub> nanocomposite coatings on 316 stainless steel. *Surf. Coat. Technol.* **339**, 199 (2018).
54. **H. Wang, Y. Zheng, C. Jiang, Y. Li, and Y. Fu:** In vitro corrosion behavior and cytocompatibility of pure Fe implanted with Ta. *Surf. Coat. Technol.* **320**, 201 (2017).
55. **S.R. Kiahosseini, A. Afshar, M. Mojtahedzadeh Larijani, and M. Yousefpour:** Structural and corrosion characterization of hydroxyapatite/zirconium nitride-coated AZ91 magnesium alloy by ion beam sputtering. *Appl. Surf. Sci.* **401**, 172 (2017).
56. **M.H. Enayati, M.H. Fathi, and A. Zomorodian:** Characterisation and corrosion properties of novel hydroxyapatite niobium plasma sprayed coating. *Surf. Eng.* **25**, 338 (2009).
57. **S. Mohajernia, S. Pour-Ali, S. Hejazi, M. Saremi, and A-R. Kiani-Rashid:** Hydroxyapatite coating containing multi-walled carbon nanotubes on AZ31 magnesium: Mechanical-electrochemical degradation in a physiological environment. *Ceram. Int.* **44**, 8297 (2018).
58. **Y.W. Gu, K.A. Khor, and P. Cheang:** In vitro studies of plasma-sprayed hydroxyapatite/Ti–6Al–4V composite coatings in simulated body fluid (SBF). *Biomaterials* **24**, 1603 (2003).
59. **C.Y. Yang, B.C. Wang, E. Chang, and B.C. Wu:** Bond degradation at the plasma-sprayed HA coating/Ti–6Al–4V alloy interface: An in vitro study. *J. Mater. Sci.: Mater. Med.* **6**, 258 (1995).
60. **Z. Zhang, M.F. Dunn, T.D. Xiao, A.P. Tomsia, and E. Saiz:** Nanostructured hydroxyapatite coatings for improved adhesion and corrosion resistance for medical implants. *MRS Online Proc. Libr.* **703**, 291 (2001).
61. **K. Balani, R. Anderson, T. Laha, M. Andara, J. Tercero, E. Crumpler, and A. Agarwal:** Plasma-sprayed carbon nanotube reinforced hydroxyapatite coatings and their interaction with human osteoblasts in vitro. *Biomaterials* **28**, 618 (2007).